# Thermodynamic Analysis of the Phase Equilibria in the Nb-Ni-Zr System[*1]

Tatsuya Tokunaga[1,*2], Satoshi Matsumoto[2,*3], Hiroshi Ohtani[3,*4] and Mitsuhiro Hasebe[3]

[1]*Core Research for Evolutional Science and Technology (CREST), Japan Science and Technology Agency (JST), Kitakyushu 804-8550, Japan*
[2]*Graduate School of Engineering, Kyushu Institute of Technology, Kitakyushu 804-8550, Japan*
[3]*Department of Materials Science and Engineering, Kyushu Institute of Technology, Kitakyushu 804-8550, Japan*

A thermodynamic study of phase equilibria in the Nb-Ni-Zr system has been carried out experimentally and using the CALPHAD method. To enable the thermodynamic description of the constituent binary systems, the results from a previous evaluation were adopted for the Nb-Ni, Ni-Zr and Nb-Zr systems. However, some modifications of the thermodynamic parameters of the Ni-Zr system were made based on recent experimental data on the binary and ternary phase equilibria. The phase boundaries involving the liquid phase in the Nb-Ni-Zr ternary system at the constant 60 mol%Ni and 20 mol%Zr were determined experimentally using differential scanning calorimetry (DSC). The thermodynamic parameters of the Nb-Ni-Zr ternary system were evaluated by combining the experimental results from DSC with reported phase boundaries of the isothermal sections at 773 and 1073 K. The calculated results reproduced the DSC results as well as the experimental isothermal sections. Furthermore, the amorphous-forming ability of Nb-Ni-Zr ternary alloys was evaluated by incorporating the thermodynamic properties from the phase diagram calculations into the Davies-Uhlmann kinetic formulations. The calculated critical cooling rates in the observed metallic glass forming compositional range were found to be lower than those in the observed amorphous forming range by one or more orders of magnitude. [doi:10.2320/matertrans.MB200713]

(Received March 19, 2007; Accepted April 6, 2007; Published August 25, 2007)

*Keywords: phase diagram, thermodynamic analysis, liquidus surface, amorphous-forming ability, critical cooling rate, calculation of phase diagrams (CALPHAD)*

## 1. Introduction

In the Nb-Ni-Zr system, amorphous or glassy alloys form over a wide composition range,[1] and these non-crystalline alloys are expected to act as membrane materials for hydrogen purification due to their high hydrogen permeability.[2,3] Although the amorphous- or glassy-forming ability (hereafter referred to as "amorphous-forming ability") is relevant to the liquidus temperatures, information on the phase equilibria of this ternary system is limited in the solid state, such as the isothermal sections at 773 and 1073 K,[4–6] and the phase equilibria involving the liquid phase is not clear.

To elucidate the phase equilibria involving the liquid phase, we have examined the phase boundaries at the 60 mol%Ni and 20 mol%Zr sections using differential scanning calorimetry (DSC), and a thermodynamic analysis of the Nb-Ni-Zr ternary system has been carried out by combining the experimental DSC results with literature data using the Calculation of Phase Diagrams (CALPHAD) method.[7]

In addition to the phase diagrams, quantitative information on the amorphous-forming ability of Nb-Ni-Zr alloys is useful for understanding their thermal stability and for further development of these hydrogen permeable membrane materials. In this study, the amorphous-forming ability has also been evaluated in terms of the critical cooling rate for amorphous formation, by incorporating the thermodynamic quantities obtained from the phase diagram calculations into the Davies-Uhlmann kinetic formulations.[8]

## 2. Experimental Procedures

The alloys used in the DSC measurements were prepared from pure Nb (99.9%) and Ni (99.9%) powders and a pure Zr (99.6%) sponge using the following procedures. Initially, the Nb-Ni alloys were obtained by arc melting cold-pressed pellets of Nb-Ni mixed powders in an argon atmosphere, and then these alloys were melted together with the Zr sponge in the same way. The arc-melted alloys were remelted in a high-frequency induction furnace for homogenization. The chemical compositions of the samples were analysed using inductively coupled plasma (ICP) atomic emission spectroscopy (Model ICP1000V, Shimadzu Corporation, Kyoto, Japan). The phase boundaries of the Nb-Ni-Zr ternary system at the 60 mol%Ni and 20 mol%Zr sections were investigated using DSC (Model EXSTAR6300, Seiko Instruments Inc., Chiba, Japan). The samples were heated and cooled at a rate of 5 K/min under flowing argon during the DSC measurements using an $\alpha$-Al$_2$O$_3$ reference standard. The peak temperature values during heating were adopted in our thermodynamic analysis to avoid any experimental errors caused by supercooling. The peak temperatures during heating are shown in Table 1.

## 3. Thermodynamic Modelling

The Gibbs energy for the individual phases was described using the regular solution approximation[9] or sublattice

Table 1 The experimental phase boundaries of Nb-Ni-Zr ternary alloys determined on heating using a DSC.

| | Alloy compositions (mass%) | | | Alloy compositions (mol%) | | | Peak temperature (K) | |
|---|---|---|---|---|---|---|---|---|
| | Nb | Ni | Zr | Nb | Ni | Zr | | |
| 60Ni series | 47.1 | 50.3 | 2.6 | 36.4 | 61.6 | 2.0 | 1452 | |
| | 39.8 | 50.3 | 9.9 | 30.7 | 61.5 | 7.8 | 1424 | |
| | 33.0 | 50.2 | 16.8 | 25.5 | 61.3 | 13.2 | 1400 | |
| | 26.4 | 49.8 | 13.8 | 20.4 | 60.9 | 18.7 | 1391 | |
| | 12.7 | 47.6 | 39.7 | 9.9 | 58.6 | 31.5 | 1403 | |
| | 6.8 | 50.1 | 43.1 | 5.3 | 61.0 | 33.7 | 1385 | |
| 20Zr series | 42.2 | 34.2 | 23.6 | 35.0 | 45.0 | 20.0 | 1391 | |
| | 36.2 | 38.4 | 25.4 | 29.5 | 49.5 | 21.0 | 1399 | |
| | 32.0 | 44.4 | 23.6 | 25.3 | 55.6 | 21.1 | 1399 | |
| | 26.5 | 49.7 | 23.8 | 20.5 | 60.8 | 18.7 | 1384 | |
| | 20.4 | 55.1 | 24.5 | 15.4 | 65.8 | 18.8 | 1386 | |
| | 13.9 | 60.4 | 25.7 | 10.2 | 70.5 | 19.3 | 1380 | 1518 |
| | 7.2 | 66.4 | 26.4 | 5.2 | 75.5 | 19.3 | 1571 | |

model.[10] A description of the Gibbs energy for each phase appearing in the Nb-Ni-Zr ternary system will be presented in this section.

The regular solution approximation was applied to the liquid and primary solid solution phases. The Gibbs energy of the $\phi$ phase was described using the following equation:

$$
\begin{aligned}
G_m^\phi = {} & x_{Nb}{}^\circ G_{Nb}^\phi + x_{Ni}{}^\circ G_{Ni}^\phi + x_{Zr}{}^\circ G_{Zr}^\phi \\
& + RT(x_{Nb} \ln x_{Nb} + x_{Ni} \ln x_{Ni} + x_{Zr} \ln x_{Zr}) \\
& + x_{Nb}x_{Ni}L_{Nb,Ni}^\phi + x_{Nb}x_{Zr}L_{Nb,Zr}^\phi + x_{Ni}x_{Zr}L_{Ni,Zr}^\phi \\
& + x_{Nb}x_{Ni}x_{Zr}L_{Nb,Ni,Zr}^\phi
\end{aligned} \tag{1}
$$

where $x_i$ denotes the mole fraction of element $i$, $R$ is the universal gas constant, and $T$ is temperature in Kelvin. The term $^\circ G_i^\phi$ denotes the Gibbs energy of element $i$ in the $\phi$ phase, and is called the lattice stability parameter. This value is described as a function of the temperature, $T$, by the formula:

$$
\begin{aligned}
^\circ G_i^\phi - {}^\circ H_i^{ref} = {} & A + BT + CT \ln T + DT^2 + ET^3 + FT^7 \\
& + IT^{-1} + JT^{-9}
\end{aligned} \tag{2}
$$

where $^\circ H_i^{ref}$ denotes the molar enthalpy of the pure element $i$ in its stable state at $T = 298$ K for the lattice stability parameter. The symbols $A$ to $J$ denote coefficients. The parameter $L_{i,j}^\phi$ denotes the interaction energy between $i$ and $j$ in the $\phi$ phase, and has a compositional dependency using an $n$th degree Redlich-Kister polynomial[11] as follows:

$$
\begin{aligned}
L_{i,j}^\phi = {} & {}^0L_{i,j}^\phi + {}^1L_{i,j}^\phi(x_i - x_j) + {}^2L_{i,j}^\phi(x_i - x_j)^2 \\
& + \cdots + {}^nL_{i,j}^\phi(x_i - x_j)^n
\end{aligned} \tag{3}
$$

where:

$$
{}^nL_{i,j}^\phi = a + bT + cT \ln T + dT^2 + \cdots. \tag{4}
$$

The term $L_{Nb,Ni,Zr}^\phi$ is the ternary interaction parameter between Nb, Ni, and Zr. The compositional dependency of this parameter is expressed as follows:

$$
L_{Nb,Ni,Zr}^\phi = x_{Nb}{}^0L_{Nb,Ni,Zr}^\phi + x_{Ni}{}^1L_{Nb,Ni,Zr}^\phi + x_{Zr}{}^2L_{Nb,Ni,Zr}^\phi. \tag{5}
$$

The Gibbs energy contribution due to ferromagnetic or-

dering of the Ni-rich fcc solid solution phase ($(\gamma)$) was described using the equation of Hillert and Jarl[12,13] as follows:

$$
G_{mag}^\gamma = RTf(\tau) \ln(\beta + 1) \tag{6}
$$

where $G_{mag}^\gamma$ is the Gibbs energy of the magnetic ordering, $\beta$ is the average magnetic moment per atom expressed in Bohr magnetons, and $f(\tau)$ is a polynomial function of $\tau$. The term $\tau$ is defined as $\tau = T/T_C$, where $T_C$ is the Curie temperature.

The Gibbs energy of compound phases with some homogeneity range was described using the sublattice model. For the simple case of a phase with the formula $(A,B)_m(C,D)_n$, where $m$ and $n$ are the numbers of the sites of Sublattice 1 and Sublattice 2, respectively, the Gibbs energy per mole of atoms of the compound is given by:

$$
\begin{aligned}
G_m = {} & y_A^1 y_C^2 {}^\circ G_{A:C} + y_B^1 y_C^2 {}^\circ G_{B:C} + y_A^1 y_D^2 {}^\circ G_{A:D} \\
& + y_B^1 y_D^2 {}^\circ G_{B:D} + mRT(y_A^1 \ln y_A^1 + y_B^1 \ln y_B^1) \\
& + nRT(y_C^2 \ln y_C^2 + y_D^2 \ln y_D^2) + {}^{ex}G
\end{aligned} \tag{7}
$$

where $^\circ G_{A:C}$ denotes the Gibbs energy of a hypothetical compound, $A_mC_n$, in which all the sites in Sublattice 1 are occupied by Element A, and all the sites in Sublattice 2 are occupied by Element C. The colon separates the constituent elements in the sublattice. The site fraction of the elements on the $s$th sublattice is denoted by $y_i^s$. The term $^{ex}G$ is the excess Gibbs energy term containing the interaction energy between unlike atoms and is expressed by the following equation:

$$
\begin{aligned}
^{ex}G = {} & y_A^1 y_B^1 y_C^2 L_{A,B:C} + y_A^1 y_B^1 y_D^2 L_{A,B:D} \\
& + y_C^2 y_D^2 y_A^1 L_{A:C,D} + y_C^2 y_D^2 y_B^1 L_{B:C,D}
\end{aligned} \tag{8}
$$

where $L_{i,j:k}$ (or $L_{i:j,k}$) is the interaction parameter between unlike atoms on the same sublattice, and is described by an equation similar to eq. (3).

In this analysis, the formulae $(Nb,Ni)_{0.25}(Nb,Ni)_{0.75}$, $(Nb,Ni)_{0.4615}(Nb,Ni)_{0.5385}$, $(Ni,Zr)_{0.833}(Va,Zr)_{0.167}$, $(Ni,Zr)_{0.75}$-$(Va,Zr)_{0.25}$, and $(Ni,Zr)_{0.575}(Va,Zr)_{0.425}$ were adopted for the compound phases, $NbNi_3$, $Nb_6Ni_7$, $Ni_5Zr$, $Ni_3Zr$, and $Ni_{10}Zr_7$, respectively, where Va denotes a vacancy.

The remaining phases were treated as being stoichiometric compounds. For example, the Gibbs energy of the $Ni_{21}Zr_8$ phase was described as follows:

$$
G_{Ni:Zr}^{Ni_{21}Zr_8} - 0.725^\circ G_{Ni}^\gamma - 0.275^\circ G_{Zr}^\beta = a + bT \tag{9}
$$

where the terms $a$ and $b$ correspond to the enthalpy and entropy terms, respectively, and were evaluated in this study.

## 4. Kinetic Formulations

The amorphous-forming ability of alloys can be characterized in terms of the critical cooling rate to avoid nucleation and growth of a crystalline phase during continuous cooling from a supercooled liquid. In this study, we obtained the critical cooling rate for amorphous formation using the kinetic formulations derived by Davies[14] and Uhlmann[15] for the time-temperature-transformation (TTT) curve, based on Johnson-Mehl-Avrami isothermal transformation kinetics for steady-state homogeneous nucleation.[16] In the Davies-Uhlmann kinetic formulations, the time, $t$, necessary for the formation of a crystalline phase of volume fraction, $X$, is given by the following equation:

Table 2 The alloy compositions used in our calculations, along with the glass transition temperatures, primary crystalline phases controlling amorphization, and the calculated critical cooling rates of Nb-Ni-Zr ternary alloys.

| No. | Alloy compositions (mol%) | | | $T_g$ (K) | Phase | $R_c$ (K/s) |
|-----|------|------|------|-----------|-------|-------------|
| | Nb | Ni | Zr | | | |
| 1 | 0 | 80 | 20 | 762* | $Ni_7Zr_2$ | $3.4 \times 10^9$ |
| 2 | 20 | 80 | 0 | 723* | $NbNi_3$ | $1.1 \times 10^8$ |
| 3 | 0 | 70 | 30 | 813* | $Ni_7Zr_2$ | $8.7 \times 10^7$ |
| 4 | 30 | 70 | 0 | 824* | $NbNi_3$ | $4.2 \times 10^6$ |
| 5 | 0 | 65 | 35 | 832[21] | $Ni_{21}Zr_8$ | $2.1 \times 10^5$ |
| 6 | 10 | 65 | 25 | 860[1] | $Ni_{21}Zr_8$ | $2.0 \times 10^4$ |
| 7 | 15 | 65 | 20 | 865[1] | $Ni_{21}Zr_8$ | $1.2 \times 10^4$ |
| 8 | 25 | 65 | 10 | 880[1] | $NbNi_3$ | $1.7 \times 10^4$ |
| 9 | 0 | 60 | 40 | 809* | $Ni_{10}Zr_7$ | $1.4 \times 10^6$ |
| 10 | 10 | 60 | 30 | 811[1] | $Ni_{10}Zr_7$ | $3.1 \times 10^4$ |
| 11 | 20 | 60 | 20 | 839[1] | $NbNi_3$ | $5.8 \times 10^2$ |
| 12 | 30 | 60 | 10 | 870[1] | $NbNi_3$ | $5.9 \times 10^2$ |
| 13 | 40 | 60 | 0 | 896[19] | $NbNi_3$ | $6.1 \times 10^2$ |
| 14 | 15 | 55 | 30 | 795[1] | $Ni_{10}Zr_7$ | $7.5 \times 10^4$ |
| 15 | 25 | 55 | 20 | 825[1] | $Nb_6Ni_7$ | $1.8 \times 10^3$ |
| 16 | 30 | 55 | 15 | 840[1] | $Nb_6Ni_7$ | $1.9 \times 10^3$ |
| 17 | 0 | 50 | 50 | 730[22] | $NiZr$ | $3.7 \times 10^8$ |
| 18 | 10 | 50 | 40 | 770[1] | $NiZr$ | $8.6 \times 10^6$ |
| 19 | 20 | 50 | 30 | 795[1] | $NiZr$ | $1.3 \times 10^5$ |
| 20 | 30 | 50 | 20 | 820* | $Nb_6Ni_7$ | $1.7 \times 10^4$ |
| 21 | 40 | 50 | 10 | 845* | $Nb_6Ni_7$ | $3.9 \times 10^4$ |
| 22 | 50 | 50 | 0 | 935* | $Nb_6Ni_7$ | $5.3 \times 10^3$ |

* = Estimated values in this study.

$$t \approx \frac{9.3\eta}{kT} \left\{ \frac{a_0^9 X}{f^3 N_v} \frac{\exp(G^*/kT)}{[1 - \exp(-G_m/RT)]^3} \right\}^{1/4} \quad (10)$$

where $\eta$ is the viscosity of the melt, $k$ is the Boltzmann constant, $T$ is the transformation temperature, $a_0$ is the mean atomic diameter, $N_v$ is the number of atoms per unit volume, and $R$ is the universal gas constant. The fraction of sites at the liquid/crystal interface, where atoms may preferentially be added and moved, is denoted by $f$, and is given by the following expression:[15]

$$f \approx 0.2(T_m - T)/T_m \quad (11)$$

where $T_m$ is the liquidus temperature. The term $G_m$ is the molar free energy driving force for the liquid to crystallize, and $G^*$ is the free energy barrier for nucleation of a spherical nucleus.

To calculate eq. (10), it is necessary to derive the quantities $\eta$, $G_m$, and $G^*$.

The viscosity of the supercooled liquid between the glass transition temperature, $T_g$, and $T_m$ was estimated using the Doolittle expression, based on the relative free volume, $f_T$, given by the expression:[17]

$$\eta = A \exp(B/f_T) \quad (12)$$

where:

$$f_T = C \exp(-E_H/RT). \quad (13)$$

The terms $A$, $B$, and $C$ are constants, and $E_H$ is the hole formation energy. Experimental data are often unavailable,

and in this work, $E_H$ was calculated using the linear relationship between $E_H$ and $T_g$, based on a previous study of Ramachandrarao et al.[17] In addition, Ramachandrarao et al. have also shown that $f_T \approx 0.03$ and $B \approx 1$ at $T_g$. Then, assuming that $f_T = 0.03$ and $\eta = 10^{12}$ Pa·s at $T_g$, and assigning a value of $B = 1$, the other constants, $A$ and $C$ in eqs. (12) and (13), can be evaluated. Thus, if $T_g$ data are available, the viscosity of the supercooled liquid can be evaluated. The glass transition temperatures used for the evaluation of the viscosity of the binary and ternary alloys are shown in Table 2, which were estimated using the following procedure.

The experimental glass transition temperatures have been reported for Nb-Ni alloys by Jiang and Baram ($Nb_{37.6}Ni_{62.4}$)[18] and Zhang and Inoue ($Nb_{40}Ni_{60}$),[19] and for the Ni-Zr alloys by Zieliński et al. ($Ni_{100-x}Zr_x(x = 34-72)$),[20] Buschow ($Ni_{100-x}Zr_x(x = 33-77)$),[21] and Myung et al. ($Ni_{50}Zr_{50}$).[22] In this study, the glass transition temperatures for Nb-Ni and Ni-Zr alloys were calculated using the following equations obtained by fitting the experimental values to the Redlich-Kister polynomial, similar to eq. (3).[11,23]

$$T_g^{Nb-Ni} = 688x_{Nb} + 432x_{Ni} + 1500x_{Nb}x_{Ni} \quad (14)$$

$$T_g^{Ni-Zr} = 432x_{Ni} + 532x_{Zr} + x_{Ni}x_{Zr}$$
$$\times \{1140 + 1330(x_{Ni} - x_{Zr})\}. \quad (15)$$

In the above equations, the glass transition temperatures for the pure metals, Nb, Ni, and Zr were taken as 688, 432, and 532 K, respectively, using $T_g = 0.25T_m$.[18,23–25] There were variations in the experimental $T_g$ values used for the fit, and the difference between the experimental and calculated values was found to be about 50 K at most. Hence, we adopted the experimental values of $T_g$ for $Nb_{40}Ni_{60}$ (No. 13), $Ni_{75}Zr_{35}$ (No. 5), and $Ni_{50}Zr_{50}$ (No. 17) rather than the calculated values. It is noteworthy that a variation in the value of $T_g$ by 50 K changes the critical cooling rate calculated using eq. (10) by less than two orders of magnitude.

The glass transition temperatures for the ternary alloys were evaluated based on the experimental data[1] on the crystallization temperatures, $T_x$, and the supercooled liquid region, $\Delta T_x(= T_x - T_g)$. The values of $T_g$ for $Nb_{30}Ni_{50}Zr_{20}$ (No. 20) and $Nb_{40}Ni_{50}Zr_{10}$ (No. 21) were estimated assuming that $T_g$ changed linearly for a constant Ni content. In practice, the linear relationship between the value of $T_g$ and the composition was found at the 65 mol%Ni (Nos. 6–8), 60 mol%Ni (Nos. 10–12), and 55 mol%Ni (Nos. 14–16) sections, and so the above assumption was deemed to be reasonable.

The molar free energy driving force for the liquid to crystallize, $G_m$, can be obtained from the thermodynamic calculations based on the Gibbs energy functions formulated in this study, and the temperature dependence of $G_m$ was approximated as being linear using the following expression:

$$G_m = H_m^f(T_m - T)/T_m \quad (16)$$

where $H_m^f$ is the molar heat of fusion.

The free energy barrier for nucleation, $G^*$, is given by the expression:

$$G^* = \frac{16\pi}{3N}(\sigma_m^3/G_m^2) \tag{17}$$

where $N$ is Avogadro's number and $\sigma_m$ is the liquid/crystal interfacial energy per molar surface area. According to Turnbull,[26] the term $\sigma_m$ is related to the molar heat of fusion, $H_m^f$, based on the relationship between the value of the bond energy across the interface, and can be expressed as:

$$\sigma_m = \alpha H_m^f. \tag{18}$$

The constant, $\alpha$, was empirically evaluated by Saunders and Miodownik[27] to be $\alpha \sim 0.41$. Thus, the value of $G^*$ can be derived by inserting the value of $H_m^f$ into eq. (18) and then using the calculated value of $\sigma_m$ in eq. (17).

In our calculations, the constants in eq. (10) were taken to be $a_0 = 0.28 \times 10^{-9}$ m, $X = 10^{-6}$, and $N_v = 5 \times 10^{28}$ atoms/m$^3$.

Since the critical cooling rates for amorphous formation, $R_c$, can be defined as the minimum cooling speed that does not intersect the TTT curve, $R_c$ was calculated using the following equation:

$$R_c \approx \frac{T_m - T_n}{t_n} \tag{19}$$

where $T_n$ and $t_n$ are the temperature and time at the nose of the TTT curve, respectively.

## 5. Results and Discussion

In this section, the calculated phase equilibria in the binary and ternary systems will be discussed, followed by a discussion on the amorphous-forming ability of Nb-Ni-Zr ternary alloys evaluated by combining the CALPHAD and Davies-Uhlmann kinetic approaches.

In our thermodynamic analysis, the descriptions of the lattice stability parameters for each element were mostly taken from the Scientific Group Thermodata Europe (SGTE) data[28] and are shown in Table 3.

### 5.1 Thermodynamic analysis of the binary systems
### 5.1.1 The Nb-Ni binary system

The Nb-Ni binary system is composed of a liquid phase (L), a Nb-rich bcc solid solution (($\beta$ Nb)), a Ni-rich fcc solid solution (($\gamma$)), NbNi$_3$, and Nb$_6$Ni$_7$. In this binary system, the thermodynamic parameters of our previous reassessment,[29] based on the recent experimental studies of Hao and Yang,[30,31] were used, and are listed in Table 4. The calculated Nb-Ni phase diagram is shown in Fig. 1.

### 5.1.2 The Ni-Zr binary system

The following phases are known to exist in the Ni-Zr binary system: a liquid phase (L), a Ni-rich fcc solid solution (($\gamma$)), a Zr-rich hcp solid solution (($\alpha$ Zr)), a Zr-rich bcc solid solution (($\beta$ Zr)), the stoichiometric compounds, Ni$_7$Zr$_2$, Ni$_{21}$Zr$_8$, Ni$_{11}$Zr$_9$, NiZr, and NiZr$_2$, non-stoichiometric compounds, Ni$_5$Zr, Ni$_3$Zr, and Ni$_{10}$Zr$_7$.

In this binary system, the phase boundaries have been investigated over the entire composition range by Kirkpatrick and Larsen,[32] and for the Ni-rich region by Bsenko[33] and Kramer.[34] For the chemical formula of the Ni$_5$Zr$_2$ phase, designated by Kirkpatrick and Larsen, Bsenko reassigned the

stoichiometry as Ni$_{21}$Zr$_8$ with a Ni$_{21}$Hf$_8$-type crystal structure. As regards the data on the thermodynamic properties, both the enthalpy of mixing for the liquid phase[35,36] and the enthalpy of formation for the compound phases[37–40] have been reported. A critical assessment of this binary system has been carried out by Nash and Jayanth,[41] and a thermodynamic assessment has been reported by Saunders.[42] Ghosh[43] has performed a thermodynamic reassessment of this binary system, taking into account the formation of Ni$_3$Zr and Ni$_{11}$Zr$_9$, and the homogeneity range of Ni$_5$Zr and Ni$_{10}$Zr$_7$, which were excluded by Saunders.[42] The thermodynamic parameters assessed by Ghosh were adopted in this study. However, the phase diagram calculations showed that the homogeneity range of Ni$_3$Zr increased with decreasing temperature, reaching a value of about 10 mol% at room temperature. In addition, the experimental phase relationship concerning the phase stability of the binary compounds, for example, the phase equilibria between ($\beta$ Nb, $\beta$ Zr), NiZr, and Ni$_{10}$Zr$_7$, were not reproduced in the calculated isothermal section, based on the results of Ghosh. Thus, the thermodynamic parameters for Ni$_3$Zr were modified in such a way that the homogeneity range was less than 0.1 mol% at room temperature, and the phase stability of Ni$_{10}$Zr$_7$ and Ni$_{11}$Zr$_9$ was re-evaluated by taking into account the phase equilibria in the ternary system. This re-evaluation of the thermodynamic parameters is presumably necessary due to the fact that the parameters assessed in the thermodynamic analysis are not unique, and Hillert and Schalin[44] pointed out this non-uniqueness as a problem for a ternary extrapolation of the binary data sets.

The thermodynamic parameters are listed in Table 4, and the calculated phase diagram for the Ni-Zr binary system is shown in Fig. 2, together with the experimental data.

### 5.1.3 The Nb-Zr binary system

There are three phases with one monotectoid reaction in the Nb-Zr system: the liquid phase (L), a bcc solid solution (($\beta$ Nb, $\beta$ Zr)), and a Zr-rich hcp solid solution (($\alpha$ Zr)). A (($\beta$ #1 + $\beta$ #2)) two-phase separation is formed for the ($\beta$ Nb, $\beta$ Zr) phase.

Guillermet[45] has performed a thermodynamic analysis of this binary system, and the calculated results reproduced the experimental phase boundaries and enthalpy of formation obtained from first-principles calculations. Therefore, we adopted the thermodynamic description of Guillermet, as listed in Table 4. The calculated Nb-Zr phase diagram is shown in Fig. 3.

### 5.2 Thermodynamic analysis of the Nb-Ni-Zr ternary system and calculation of the phase diagrams

The isothermal sections of the Nb-Ni-Zr ternary system, have been reported by Evdokimova et al.[4] (1073 K), Bokii et al.[5] (1073 K) and Moraleva et al.[6] (773 and 1073 K) over the entire composition range. However, no data on the ternary compound are available in the literature. Evdokimova et al. have reported that the solubility of the third element in NbNi$_3$ and Ni$_{10}$Zr$_7$ reaches about 15 mol%Zr and 20–25 mol%Nb, respectively, whereas Bokii et al. and Moraleva et al. have shown that the solubility of the third element in all the binary compounds is less than 1 mol%. Because of the lack of the experimental verification on the identification of the ob-

Table 3 The lattice stability parameters of Nb, Ni, and Zr.

| Element | Phase | Lattice stability parameters (J/mol) | | Temperature (K) | Reference |
|---|---|---|---|---|---|
| Nb | $\beta$ | $°G_{Nb}^{\beta} - °H_{Nb}^{\beta}$ | $= -8519.353 + 142.045475T - 26.4711T \ln T$ $+2.03475 \times 10^{-4}T^2 - 3.5012 \times 10^{-7}T^3 + 93399T^{-1}$ | $298 < T < 2750$ | 28) |
| | | | $= -37669.3 + 271.720843T - 41.77T \ln T + 1.528238 \times 10^{32}T^{-9}$ | $2750 < T < 6000$ | |
| | $\gamma$ | $°G_{Nb}^{\gamma} - °G_{Nb}^{\beta}$ | $= +13500 + 1.7T$ | $298 < T < 6000$ | |
| | $\alpha Zr$ | $°G_{Nb}^{\alpha Zr} - °G_{Nb}^{\beta}$ | $= +10000 + 2.4T$ | $298 < T < 6000$ | |
| | NbNi$_3$ | $°G_{Nb:Nb}^{NbNi_3} - °G_{Nb}^{\beta}$ | $= +5000$ | $298 < T < 6000$ | 29) |
| | Nb$_6$Ni$_7$ | $°G_{Nb:Nb}^{Nb_6Ni_7} - °G_{Nb}^{\beta}$ | $= +9840$ | $298 < T < 6000$ | |
| | L | $°G_{Nb}^{L} - °G_{Nb}^{\beta}$ | $= +29781.555 - 10.816418T - 3.06098 \times 10^{-23}T^7$ | $298 < T < 2750$ | 28) |
| | | | $= +30169.902 - 10.964695T - 1.528238 \times 10^{32}T^{-9}$ | $2750 < T < 6000$ | |
| Ni | $\beta$ | $°G_{Ni}^{\beta} - °G_{Ni}^{\gamma}$ | $= +8715.084 - 3.556T$ | $298 < T < 3000$ | 28) |
| | | $T_{Ni}^{\beta} = 575, \beta_{Ni}^{\beta} = 0.85$ | | $298 < T < 3000$ | |
| | $\gamma$ | $°G_{Ni}^{\gamma} - °H_{Ni}^{\gamma}$ | $= -5179.159 + 117.854T - 22.096T \ln T - 0.0048407T^2$ | $298 < T < 1728$ | |
| | | | $= -27840.655 + 279.135T - 43.1T \ln T + 1.12754 \times 10^{31}T^{-9}$ | $1728 < T < 3000$ | |
| | | $T_{Ni}^{\gamma} = 633, \beta_{Ni}^{\gamma} = 0.52$ | | $298 < T < 3000$ | |
| | $\alpha Zr$ | $°G_{Ni}^{\alpha Zr} - °G_{Ni}^{\gamma}$ | $= +1046 + 1.255T$ | $298 < T < 3000$ | |
| | | $T_{Ni}^{\alpha Zr} = 633, \beta_{Ni}^{\alpha Zr} = 0.52$ | | $298 < T < 6000$ | |
| | NbNi$_3$ | $°G_{Ni:Ni}^{NbNi_3} - °G_{Ni}^{\gamma}$ | $= +5000$ | $298 < T < 6000$ | 29) |
| | Ni$_3$Zr | $°G_{Ni:Va}^{Ni_3Zr} - 0.75°G_{Ni}^{\gamma}$ | $= +10000 + 1.25T$ | $298 < T < 6000$ | 43) |
| | Ni$_5$Zr | $°G_{Ni:Va}^{Ni_5Zr} - 0.833°G_{Ni}^{\gamma}$ | $= +29566 - 8.428T$ | $298 < T < 6000$ | |
| | Ni$_{10}$Zr$_7$ | $°G_{Ni:Va}^{Ni_{10}Zr_7} - 0.575°G_{Ni}^{\gamma}$ | $= +20051 - 5.8167T$ | $298 < T < 6000$ | |
| | L | $°G_{Ni}^{L} - °H_{Ni}^{\gamma}$ | $= +11235.527 + 108.457T - 22.096T \ln T$ $-0.0048407T^2 - 3.82318 \times 10^{-21}T^7$ | $298 < T < 1728$ | 28) |
| | | | $= -9549.775 + 268.598T - 43.1T \ln T$ | $1728 < T < 3000$ | |
| Zr | $\beta$ | $°G_{Zr}^{\beta} - °H_{Zr}^{\alpha Zr}$ | $= -525.539 + 124.9457T - 25.607406T \ln T - 3.40084 \times 10^{-4}T^2$ $-9.729 \times 10^{-9}T^3 + 25233T^{-1} - 7.6143 \times 10^{-11}T^4$ | $298 < T < 2128$ | 28) |
| | | | $= -30705.955 + 264.284163T - 42.144T \ln T + 1.276058 \times 10^{32}T^{-9}$ | $2128 < T < 6000$ | |
| | $\gamma$ | $°G_{Zr}^{\gamma} - °G_{Zr}^{\alpha Zr}$ | $= +7600 - 0.9T$ | $298 < T < 6000$ | |
| | $\alpha Zr$ | $°G_{Zr}^{\alpha Zr} - °H_{Zr}^{\alpha Zr}$ | $= -7827.595 + 125.64905T - 24.1618T \ln T$ $-0.00437791T^2 + 34971T^{-1}$ | $298 < T < 2128$ | |
| | | | $= -26085.921 + 262.724183T - 42.144T \ln T - 1.342896 \times 10^{31}T^{-9}$ | $2128 < T < 6000$ | |
| | Ni$_3$Zr | $°G_{Zr:Zr}^{Ni_3Zr} - °G_{Zr}^{\beta}$ | $= 0$ | $298 < T < 6000$ | 43) |
| | | $°G_{Zr:Va}^{Ni_3Zr} - 0.75°G_{Zr}^{\beta}$ | $= +47425 + 5.68T$ | | |
| | Ni$_5$Zr | $°G_{Zr:Zr}^{Ni_5Zr} - °G_{Zr}^{\beta}$ | $= +7600 - 0.9T$ | $298 < T < 6000$ | |
| | | $°G_{Zr:Va}^{Ni_5Zr} - 0.833°G_{Zr}^{\beta}$ | $= +32493 - 8.22T$ | | |
| | Ni$_{10}$Zr$_7$ | $°G_{Zr:Zr}^{Ni_{10}Zr_7} - °G_{Zr}^{\beta}$ | $= +8750 - 2.556T$ | $298 < T < 6000$ | |
| | | $°G_{Zr:Va}^{Ni_{10}Zr_7} - 0.575°G_{Zr}^{\beta}$ | $= +22075 - 5.674T$ | | |
| | L | $°G_{Zr}^{L} - °G_{Zr}^{\alpha Zr}$ | $= +18147.69 - 9.080812T + 1.6275 \times 10^{-22}T^7$ | $298 < T < 2128$ | 28) |
| | | | $= +17804.661 - 8.911574T + 1.342895 \times 10^{31}T^{-9}$ | $2128 < T < 6000$ | |

served phases and determination of the phase boundaries,[46] all the binary compound phases were treated as being pure binary phases in this study. The ternary thermodynamic parameters were evaluated based on our experimental DSC data, together with the experimental isothermal sections of Bokii et al.[5] and Moraleva et al.[6] The optimized thermodynamic parameters are listed in Table 4.

The calculated isothermal section diagrams at 773 and 1073 K were compared with the experimental results,[6] as shown in Figs. 4(a) and 4(b), respectively. For the bcc phase, ($\beta$), Bokii et al. showed that the solubility of Ni was negligible, whereas Moraleva et al. estimated the solubility of Ni to be 2–3 mol%. However, we could not obtain the ternary parameters for the bcc phase, ($\beta$), that fitted the experimental results of Moraleva et al., and thus, the ternary thermodynamic parameters for this phase were not taken into

account in this study.

Figures 5(a) and 5(b) show the calculated vertical section diagrams at 60 mol%Ni and 20 mol%Zr, respectively, along with the DSC results. In this analysis, the parameter, $^1L_{Nb,Ni,Zr}^{L}$, in eq. (5) was optimized using the DSC data. However, the optimized parameter could not reproduce the experimental liquidus temperatures at a composition of 31.5 mol%Zr in Fig. 5(a) and 65.8 mol%Ni in Fig. 5(b).

The calculated liquidus surface projection is shown in Fig. 6. The liquidus surface of the Nb-Ni-Zr ternary system was composed of a primary crystallization region: ($\beta$), ($\gamma$), NbNi$_3$, Nb$_6$Ni$_7$, Ni$_7$Zr$_2$, Ni$_{21}$Zr$_8$, Ni$_{11}$Zr$_9$, NiZr, NiZr$_2$, Ni$_5$Zr, and Ni$_{10}$Zr$_7$, along with 10 types of ternary invariant reactions, as summarized in Table 5. The letters E and U in Table 5 denote the ternary eutectic and peritectic reactions, respectively. Except for Point E$_4$, the ternary eutectic

Table 4　The optimized thermodynamic parameters of the Nb-Ni-Zr system.

| System | Phase | Thermodynamic parameters (J/mol) | Reference |
|---|---|---|---|
| Nb-Ni | $\beta$ | $L^{\beta}_{\text{Nb,Ni}} = -33500 + 10T$ | 29) |
| | $\gamma$ | $L^{\gamma}_{\text{Nb,Ni}} = -70007.4 - 7.39665T + (96115 - 23.07497T) \cdot (x_{\text{Nb}} - x_{\text{Ni}})$ | |
| | | $T^{\gamma}_{\text{C(Nb,Ni)}} = -1200 + 760 \cdot (x_{\text{Nb}} - x_{\text{Ni}})$ | |
| | NbNi$_3$ | $^{\circ}G^{\text{NbNi}_3}_{\text{Nb:Ni}} - 0.25^{\circ}G^{\beta}_{\text{Nb}} - 0.75^{\circ}G^{\gamma}_{\text{Ni}} = -35300.6 + 4.83322T$ | |
| | | $^{\circ}G^{\text{NbNi}_3}_{\text{Ni:Nb}} - 0.25^{\circ}G^{\gamma}_{\text{Ni}} - 0.75^{\circ}G^{\beta}_{\text{Nb}} = +45300.575 - 4.83322T$ | |
| | | $L^{\text{NbNi}_3}_{\text{Nb,Ni:Nb}} = L^{\text{NbNi}_3}_{\text{Nb,Ni:Ni}} = -3079.625$ | |
| | | $L^{\text{NbNi}_3}_{\text{Nb:Nb,Ni}} = L^{\text{NbNi}_3}_{\text{Ni:Nb,Ni}} = +13505.625$ | |
| | Nb$_6$Ni$_7$ | $^{\circ}G^{\text{Nb}_6\text{Ni}_7}_{\text{Nb:Ni}} - 0.4615^{\circ}G^{\beta}_{\text{Nb}} - 0.5385^{\circ}G^{\gamma}_{\text{Ni}} = -22770 + 0.305T$ | |
| | | $L^{\text{Nb}_6\text{Ni}_7}_{\text{Nb:Nb,Ni}} = +6850 + 26460 \cdot (y^2_{\text{Nb}} - y^2_{\text{Ni}})$ | |
| | L | $L^{\text{L}}_{\text{Nb,Ni}} = -80037.3 - 6.31498T + (97884.9 - 19.01069T) \cdot (x_{\text{Nb}} - x_{\text{Ni}}) + 10000 \cdot (x_{\text{Nb}} - x_{\text{Ni}})^2$ | |
| Ni-Zr | $\beta$ | $L^{\beta}_{\text{Ni,Zr}} = -147500 + 2.3T + (-43500 - 11.6T) \cdot (x_{\text{Ni}} - x_{\text{Zr}})$ | 43) |
| | $\gamma$ | $L^{\gamma}_{\text{Ni,Zr}} = -130000 + 2T + (-25000 + 2.5T) \cdot (x_{\text{Ni}} - x_{\text{Zr}})$ | |
| | $\alpha$Zr | $L^{\alpha\text{Zr}}_{\text{Ni,Zr}} = -68350 + 3.5T + (10000 - 6.6T) \cdot (x_{\text{Ni}} - x_{\text{Zr}})$ | |
| | NiZr | $^{\circ}G^{\text{NiZr}}_{\text{Ni:Zr}} - 0.5^{\circ}G^{\gamma}_{\text{Ni}} - 0.5^{\circ}G^{\beta}_{\text{Zr}} = -52275 + 0.6T$ | |
| | NiZr$_2$ | $^{\circ}G^{\text{NiZr}_2}_{\text{Ni:Zr}} - 0.333^{\circ}G^{\gamma}_{\text{Ni}} - 0.667^{\circ}G^{\beta}_{\text{Zr}} = -40650 + 0.15T$ | |
| | Ni$_3$Zr | $^{\circ}G^{\text{Ni}_3\text{Zr}}_{\text{Ni:Zr}} - 0.75^{\circ}G^{\gamma}_{\text{Ni}} - 0.25^{\circ}G^{\beta}_{\text{Zr}} = -43410 + 0.88T$ | Present work |
| | | $L^{\text{Ni}_3\text{Zr}}_{\text{Ni:Va,Zr}} = -25000 + 4.5T$ | |
| | | $L^{\text{Ni}_3\text{Zr}}_{\text{Ni,Zr:Va}} = +75500$ | 43) |
| | | $L^{\text{Ni}_3\text{Zr}}_{\text{Ni,Zr:Zr}} = +7555$ | |
| | Ni$_5$Zr | $^{\circ}G^{\text{Ni}_5\text{Zr}}_{\text{Ni:Zr}} - 0.833^{\circ}G^{\gamma}_{\text{Ni}} - 0.167^{\circ}G^{\beta}_{\text{Zr}} = -33205 + 0.95T$ | |
| | | $L^{\text{Ni}_5\text{Zr}}_{\text{Ni:Va,Zr}} = -19475 + 1.25T$ | |
| | | $L^{\text{Ni}_5\text{Zr}}_{\text{Ni,Zr:Va}} = +76500$ | |
| | | $L^{\text{Ni}_5\text{Zr}}_{\text{Ni,Zr:Zr}} = +7850$ | |
| | Ni$_7$Zr$_2$ | $^{\circ}G^{\text{Ni}_7\text{Zr}_2}_{\text{Ni:Zr}} - 0.78^{\circ}G^{\gamma}_{\text{Ni}} - 0.22^{\circ}G^{\beta}_{\text{Zr}} = -40775 + 0.3T$ | |
| | Ni$_{10}$Zr$_7$ | $^{\circ}G^{\text{Ni}_{10}\text{Zr}_7}_{\text{Ni:Zr}} - 0.575^{\circ}G^{\gamma}_{\text{Ni}} - 0.425^{\circ}G^{\beta}_{\text{Zr}} = -53000 + 1.75T$ | Present work |
| | | $L^{\text{Ni}_{10}\text{Zr}_7}_{\text{Ni:Va,Zr}} = -19250$ | 43) |
| | | $L^{\text{Ni}_{10}\text{Zr}_7}_{\text{Ni,Zr:Va}} = +56000$ | |
| | | $L^{\text{Ni}_{10}\text{Zr}_7}_{\text{Ni,Zr:Zr}} = +8500$ | |
| | Ni$_{11}$Zr$_9$ | $^{\circ}G^{\text{Ni}_{11}\text{Zr}_9}_{\text{Ni:Zr}} - 0.55^{\circ}G^{\gamma}_{\text{Ni}} - 0.45^{\circ}G^{\beta}_{\text{Zr}} = -52000 + 0.74T$ | Present work |
| | Ni$_{21}$Zr$_8$ | $^{\circ}G^{\text{Ni}_{21}\text{Zr}_8}_{\text{Ni:Zr}} - 0.725^{\circ}G^{\gamma}_{\text{Ni}} - 0.275^{\circ}G^{\beta}_{\text{Zr}} = -44625 + 0.5T$ | 43) |
| | L | $L^{\text{L}}_{\text{Ni,Zr}} = -200450 + 10.35T + (-42925 + 3.58T) \cdot (x_{\text{Ni}} - x_{\text{Zr}}) + (-34000 + 32.37T) \cdot (x_{\text{Ni}} - x_{\text{Zr}})^2$ | |
| Nb-Zr | $\beta$ | $L^{\beta}_{\text{Nb,Zr}} = +15911 + 3.35T + (3919 - 1.091T) \cdot (x_{\text{Nb}} - x_{\text{Zr}})$ | 45) |
| | $\alpha$Zr | $L^{\alpha\text{Zr}}_{\text{Nb,Zr}} = +24411$ | |
| | L | $L^{\text{L}}_{\text{Nb,Zr}} = +10311 + 6709 \cdot (x_{\text{Nb}} - x_{\text{Zr}})$ | |
| Nb-Ni-Zr | L | $L^{\text{L}}_{\text{Nb,Ni,Zr}} = +240000 \cdot x_{\text{Ni}}$ | Present work |
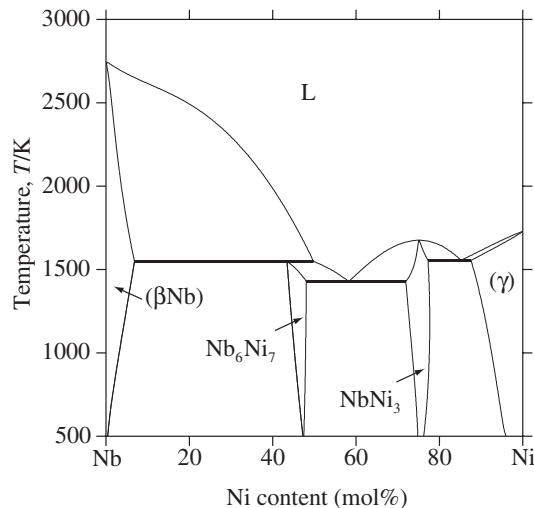


Fig. 1　The calculated binary phase diagram of the Nb-Ni system.
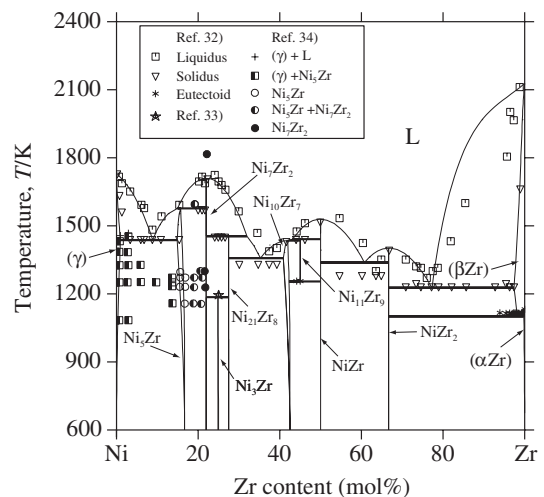


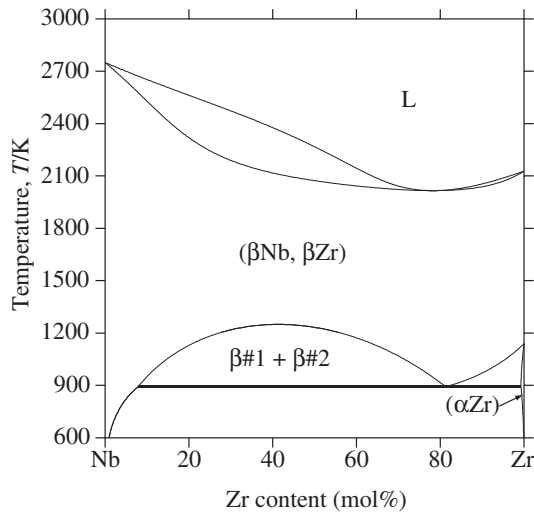Fig. 2　The calculated binary phase diagram of the Ni-Zr system.

Fig. 3  The calculated binary phase diagram of the Nb-Zr system.

reactions in the Ni-rich region occurred at relatively low temperatures. In Fig. 6, the experimental compositional range for glassy alloy formation (shaded area) and experimental boundary of the Ni-rich and Nb-Zr sides for

amorphous formation (dash-dotted lines)[1] are also shown. The compositional range where the liquidus temperatures were relatively low, including the ternary eutectic points, $E_1$ and $E_2$, are consistent with the observed compositional range for glassy alloy formation.

## 5.3  Evaluation of the amorphous-forming ability of Nb-Ni-Zr ternary alloys

The alloy composition and glass transition temperatures used in our calculation are shown in Table 2.

The calculated TTT curves for crystallization from the liquid phase of $Nb_{20}Ni_{60}Zr_{20}$ (No. 11 in Table 2), are shown in Fig. 7. According to our calculation, $NbNi_3$ controls the amorphous formation in this alloy, since the nose of the TTT curve for that compound is located at shorter times than those of the other compounds. Using eq. (19), the critical cooling rate for amorphous formation was calculated to be $5.8 \times 10^2$ K/s. The calculated critical cooling rates and the crystalline phases controlling amorphous formation in Nb-Ni-Zr ternary alloys are listed in Table 2. In Fig. 8, the calculated critical cooling rates are plotted along the calculated liquidus surface projection, together with the experimental results.[1] By considering the cooling rate of the
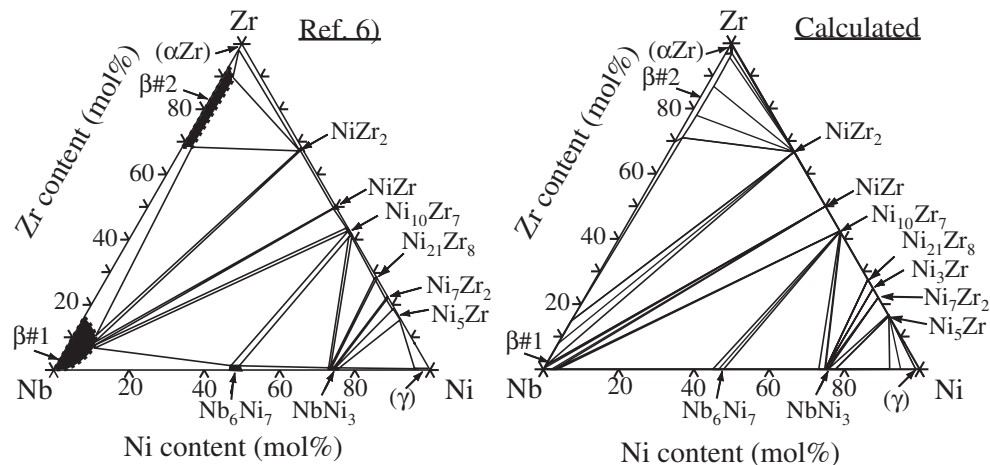
(a) 773 K
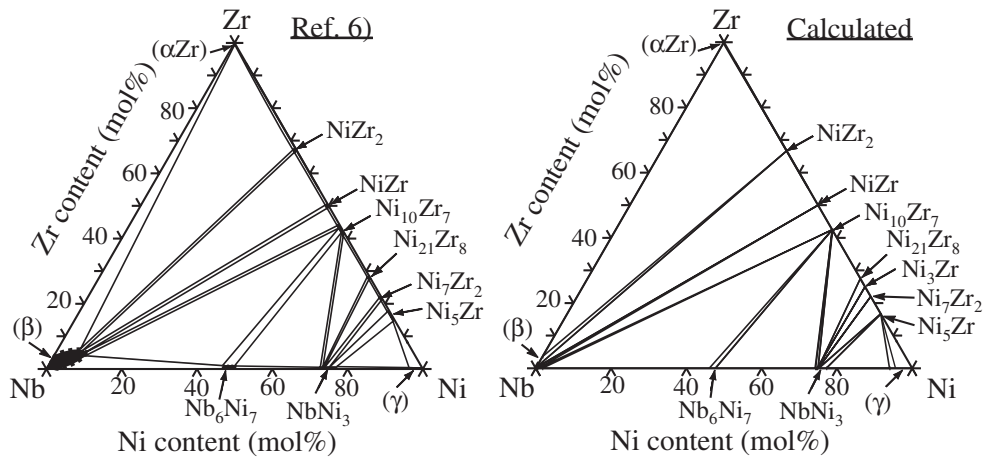


(b) 1073 K



Fig. 4  The experimental and calculated isothermal section diagrams of the Nb-Ni-Zr system at: (a) 773 K and (b) 1073 K.
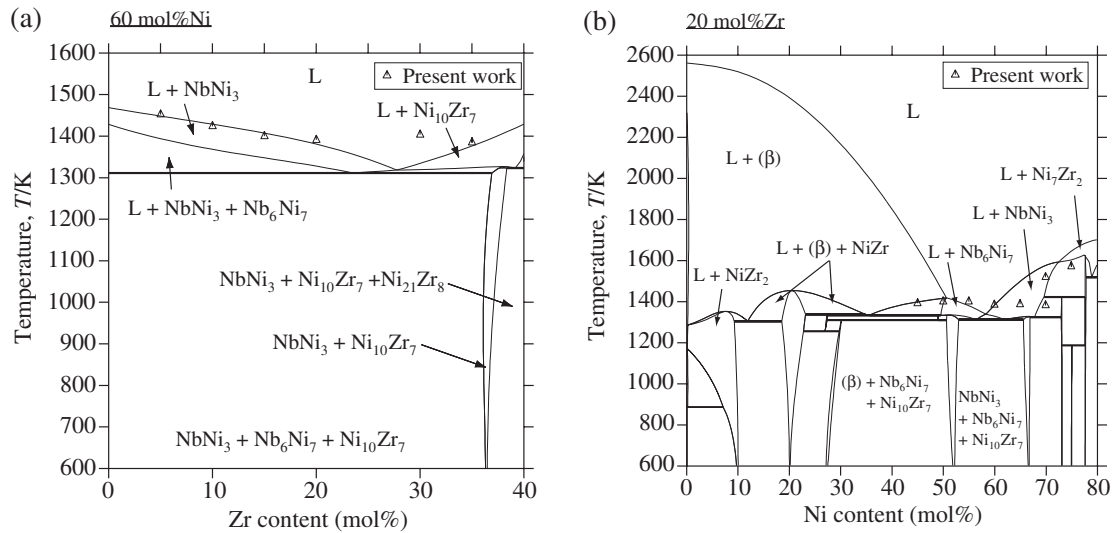
Fig. 5   Calculated vertical section diagrams of the Nb-Ni-Zr system at a constant: (a) 60 mol%Ni and (b) 20 mol%Zr.
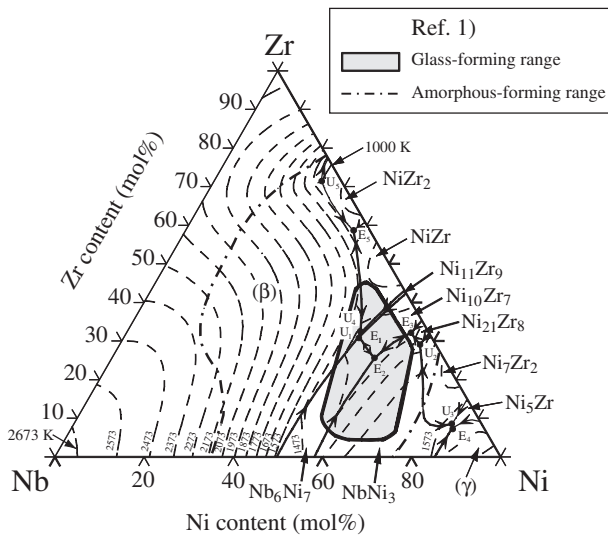


Fig. 6   The calculated liquidus surface projection of the Nb-Ni-Zr system, together with the observed glass-forming compositional range (shaded area) and boundaries for amorphous-forming (dash-dotted lines).[1]



Fig. 7   The calculated TTT curves for the crystallization of $NbNi_3$, $Nb_6Ni_7$, and $Ni_{10}Zr_7$ from liquid $Nb_{20}Ni_{60}Zr_{20}$.

Table 5   The invariant reaction points of the calculated liquidus projection.

| Type | Reaction | Temperature (K) | Composition of liquid phase (mol%) | |
|------|----------|-----------------|------|------|
| | | | Ni | Zr |
| $E_1$ | $L \Leftrightarrow Nb_6Ni_7 + Ni_{10}Zr_7 + Ni_{11}Zr_9$ | 1332 | 52.8 | 31.1 |
| $E_2$ | $L \Leftrightarrow NbNi_3 + Nb_6Ni_7 + Ni_{10}Zr_7$ | 1347 | 58.9 | 25.6 |
| $E_3$ | $L \Leftrightarrow NbNi_3 + Ni_{10}Zr_7 + Ni_{21}Zr_8$ | 1323 | 63.8 | 32.1 |
| $E_4$ | $L \Leftrightarrow (\gamma) + NbNi_3 + Ni_5Zr$ | 1509 | 85.4 | 7.5 |
| $E_5$ | $L \Leftrightarrow (\beta) + NiZr + NiZr_2$ | 1303 | 37.6 | 58.7 |
| $U_1$ | $L + (\beta) \Leftrightarrow Nb_6Ni_7 + Ni_{11}Zr_9$ | 1332 | 52.6 | 31.2 |
| $U_2$ | $L + Ni_7Zr_2 \Leftrightarrow NbNi_3 + Ni_{21}Zr_8$ | 1421 | 67.4 | 29.1 |
| $U_3$ | $L + Ni_7Zr_2 \Leftrightarrow NbNi_3 + Ni_5Zr$ | 1517 | 84.8 | 8.5 |
| $U_4$ | $L + NiZr \Leftrightarrow (\beta) + Ni_{11}Zr_9$ | 1336 | 52.5 | 31.9 |
| $U_5$ | $L + \beta\#1 + \beta\#2 \Leftrightarrow NiZr_2$ | 1272 | 24.1 | 71.5 |

single-roller melt-spinning method employed by Kimura *et al.*[1] to be ~$10^6$ K/s,[47] there was good agreement between the calculated amorphous-forming ability and the boundary
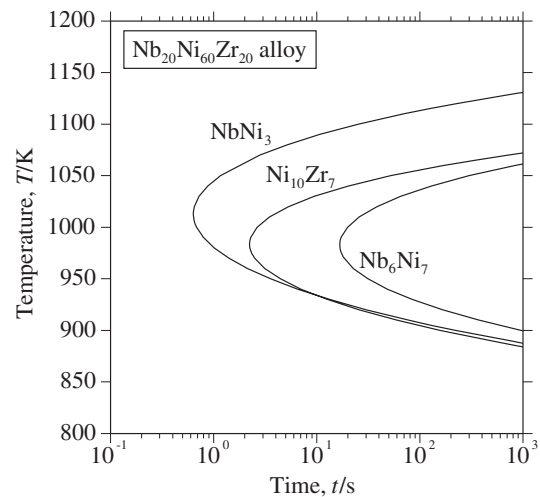
for amorphous formation on the Ni-rich side. In addition, the calculated critical cooling rates in the experimental composition range for glassy alloy formation were found to be slower than those in the composition range for amorphous formation, with the critical cooling rates for Alloys 11, 12, 15, and 16 being around $10^2$–$10^3$ K/s.

## 6.   Conclusions

A thermodynamic analysis of the Nb-Ni-Zr ternary system has been carried out based on the DSC results obtained in this study and available experimental data on the phase equilibria. Furthermore, the amorphous-forming ability of this ternary alloy was evaluated by introducing the thermodynamic quantities from the phase diagram calculations into the Davies-Uhlmann kinetic approach. The results obtained are summarized as follows:

(1)   The thermodynamic parameters of the constituent binary systems present in the Nb-Ni-Zr ternary phase diagram were taken from previous studies. However,
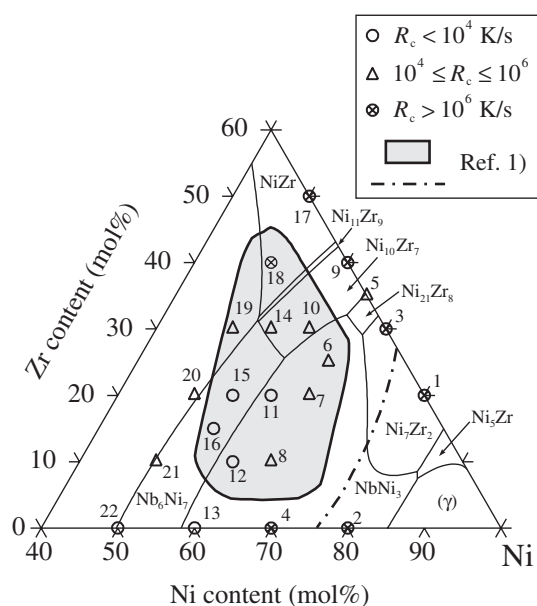
Fig. 8 A comparison of the calculated and the experimental amorphous-forming abilities of Nb-Ni-Zr ternary alloys plotted on the calculated liquidus surface projection. The numerals refer to the alloy numbers listed in Table 2. The shaded area and dash-dotted line represent the observed glass-forming compositional range and the boundaries for amorphous-forming, respectively.

some modification of the parameters for $Ni_3Zr$, $Ni_{10}Zr_7$, and $Ni_{11}Zr_9$ in the Ni-Zr binary system was attempted in this study.

(2) The ternary parameters assessed using the DSC data reproduced the experimental phase equilibria in the Nb-Ni-Zr ternary system. Our calculations reveal that 10 types of ternary invariant reactions exist in the liquidus surface of this ternary system.

(3) The calculated amorphous-forming ability agreed with the experimental results. In particular, the calculated critical cooling rates for amorphous formation were found to decrease in the order of $10^2$–$10^3$ K/s, in the experimental composition range for glassy alloy formation.

## Acknowledgement

## REFERENCES

1) H. Kimura, A. Inoue, S. Yamaura, K. Sasamori, M. Nishida, Y. Shinpo and H. Okouchi: Mater. Trans. **44** (2003) 1167–1171.
2) S. Yamaura, Y. Shinpo, H. Okouchi, M. Nishida, O. Kajita, H. Kimura and A. Inoue: Mater. Trans. **44** (2003) 1885–1890.
3) S. Yamaura, M. Sakurai, M. Hasegawa, K. Wakoh, Y. Shinpo, M. Nishida, H. Kimura, E. Matsubara and A. Inoue: Acta Mater. **53** (2005) 3703–3711.
4) A. D. Evdokimova, S. M. Kuznetsova, G. N. Ronami and E. M. Sokolovskaya: Moscow Univ. Chem. Bull., Translated from Vestnik Moscovskogo Universiteta, Khimiya, **25** (1970) 47–49.
5) G. B. Bokii, A. T. Grigor'ev, E. M. Sokolovskaya, I. G. Sokolova, V. V. Kuprina, L. A. Panteleimonov, M. V. Raevskaya, L. S. Guzei and G. N. Ronami: Metallovedenie, Struktura i Svoistva Stalei i Splavov, Metallidy Novye Metody Issledovaniya, Materialy Simpoziuma po Metallurgii Metallovedeniyu, Moscow, **1968** (1971) 311–315.
6) A. D. Moraleva, E. M. Sokolovskaya, V. V. Burnashova and V. Ya. Markiv: Moscow Univ. Chem. Bull., Translated from Vestnik Moscovskogo Universiteta, Khimiya, **23** (1968) 40–43.
7) N. Saunders and A. P. Miodownik: *CALPHAD (Calculation of Phase Diagrams): A Comprehensive Guide*, (Pergamon Materials Series, Elsevier Science Ltd, Oxford, 1998).
8) H. A. Davies: Phys. Chem. Glasses **17** (1976) 159–173.
9) J. H. Hildebrand: J. Am. Chem. Soc. **51** (1929) 66–80.
10) M. Hillert and L.-I. Staffansson: Acta Chem. Scand. **24** (1970) 3618–3626.
11) O. Redlich and A. T. Kister: Ind. Eng. Chem. **40** (1948) 345–348.
12) G. Inden: *Proc. CALPHAD V*, Düsseldorf, 1976, III-(4)-1.
13) M. Hillert and M. Jarl: CALPHAD **2** (1978) 227–238.
14) H. A. Davies: *Proc. 3rd Int. Conf. on Rapidly Quenched Metals*, ed. by B. Cantor, (The Metal Society, London, 1978) pp. 1–21.
15) D. R. Uhlmann: J. Non-Cryst. Solids **7** (1972) 337–348.
16) J. W. Christian: *The Theory of Phase Transformations in Metals and Alloys*, (Pergamon Press., Oxford, 1965) p. 377.
17) P. Ramachandrarao, B. Cantor and R. W. Cahn: J. Mater. Sci. **12** (1977) 2488–2502.
18) H. G. Jiang and J. Baram: Mater. Sci. Eng. **A208** (1996) 232–238.
19) W. Zhang and A. Inoue: Mater. Trans. **43** (2002) 2342–2345.
20) P. G. Zieliński, J. Ostatek, M. Kijek and H. Matyja: *Proc. 3rd Int. Conf. on Rapidly Quenched Metals*, ed. by B. Cantor, (The Metals Society, London, 1978) pp. 337–343.
21) K. H. J. Buschow: J. Phys. F **14** (1984) 593–607.
22) W.-N. Myung, H.-G. Kim and T. Masumoto: Mater. Sci. Eng. **A179/A180** (1994) 252–255.
23) G. Shao: J. Appl. Phys. **88** (2000) 4443–4445.
24) D. Turnbull: Contemp. Phys. **10** (1969) 473–488.
25) C. V. Thompson and F. Spaepen: Acta Metall. **31** (1983) 2021–2027.
26) D. Turnbull: J. Appl. Phys. **21** (1950) 1022–1028.
27) N. Saunders and A. P. Miodownik: Mater. Sci. Technol. **4** (1988) 768–777.
28) A. T. Dinsdale: CALPHAD **15** (1991) 317–425.
29) S. Matsumoto, T. Tokunaga, H. Ohtani and M. Hasebe: Mater. Trans. **46** (2005) 2920–2930.
30) S. Hao and G. Yang: *Proc. the 8th National Symposium on Phase Diagrams Commission on Phase Diagrams of China*, (XI'AN Northwest University, 1995) pp. 28–30.
31) G. Yang and S. Hao: J. Alloy. Compd. **297** (2000) 226–230.
32) M. E. Kirkpatrick and W. L. Larsen: Trans. ASM **54** (1961) 580–590.
33) L. Bsenko: J. Less-Common Met. **63** (1979) 171–179.
34) D. Kramer: Trans. Metall. Soc. AIME **215** (1959) 256–258.
35) O. Yu. Sidorov, Yu. O. Esin and P. V. Gel'd: Rasplavy **3** (1989) 28–33.
36) I. Arpshofen, R. Lück, B. Predel and J. F. Smith: J. Phase Equilib. **12** (1991) 141–147.
37) F. H. M. Spit, J. W. Drijver and S. Radelaar: Scri. Metall. **14** (1980) 1071–1076.
38) J. C. Gachon and J. Hertz: CALPHAD **7** (1983) 1–12.
39) M. P. Henaff, C. Colinet, A. Pasturel and K. H. J. Buschow: J. Appl. Phys. **56** (1984) 307–310.
40) J. F. Smith, Q. Jiang, R. Lück and B. Predel: J. Phase Equilib. **12** (1991) 538–545.
41) P. Nash and C. S. Jayanth: *Phase Diagrams of Binary Nickel Alloys*, ed. P. Nash, (ASM International, Materials Park, OH, USA, 1991), Monograph Series on Alloy Phase Diagrams, pp. 390–394.
42) N. Saunders: CALPHAD **9** (1985) 297–309.
43) G. Ghosh: J. Mater. Res. **9** (1994) 598–616.
44) M. Hillert and M. Schalin: J. Phase Equilib. **19** (1998) 206–212.
45) A. F. Guillermet: Z. Metallk. **82** (1991) 478–487.
46) K. P. Gupta: J. Phase Equilib. **21** (2000) 485–493.
47) U. Mizutani, Y. Hoshino and Y. Yamada: *Amorufasugoukin-sakusei-no-tebiki, —Ekitaikyurei-ho—*, (AGNE Gijutsu Center, Tokyo, 1986) p. 6 (in Japanese).